FEBS Letters

FEBS PRESS science publishing by scientists

# Mechanistic and structural studies of KDM-catalysed demethylation of histone 1 isotype 4 at lysine 26

Louise J. Walport[1], Richard J. Hopkinson[1,2], Rasheduzzaman Chowdhury[1], Yijia Zhang[1], Joanna Bonnici[1], Rachel Schiller[1], Akane Kawamura[1,3] and Christopher J. Schofield[1]

1 Department of Chemistry, Chemistry Research Laboratory, University of Oxford, UK
2 Leicester Institute of Structural and Chemical Biology and Department of Chemistry, University of Leicester, UK
3 Division of Cardiovascular Medicine, Radcliffe Department of Medicine, The Wellcome Trust Centre for Human Genetics, Oxford, UK

**Correspondence**
Christopher J. Schofield, Department of Chemistry, Chemistry Research Laboratory, University of Oxford, Mansfield Road, Oxford OX1 3TA, UK
Fax: +44 1865 285 002
Tel: +44 1865 285 006
E-mail: christopher.schofield@chem.ox.ac.uk

(Received 29 June 2018, revised 22 August 2018, accepted 24 August 2018, available online 14 September 2018)

doi:10.1002/1873-3468.13231

Edited by Miguel De la Rosa

***N*-Methylation of lysyl residues is widely observed on histone proteins. Using isolated enzymes, we report mechanistic and structural studies on histone lysine demethylase (KDM)-catalysed demethylation of $N^{\varepsilon}$-methylated lysine 26 on histone 1 isotype 4 (H1.4). The results reveal that methylated H1.4K26 is a substrate for all members of the KDM4 subfamily and that KDM4A-catalysed demethylation of H1.4K26me3 peptide is similarly efficient to that of H3K9me3. Crystallographic studies of an H1.4K26me3:KDM4A complex reveal a conserved binding geometry to that of H3K9me3. In the light of the high activity of the KDM4s on this mark, our results suggest JmjC KDM-catalysed demethylation of H1.4K26 may be as prevalent as demethylation on the H3 tail and warrants further investigation in cells.**

**Keywords:** 2-oxoglutarate oxygenases; demethylases; epigenetics; histones; JmjC demethylases; lysine *N*-methylation

Widespread *N*-methylation of both arginyl and lysyl residues occurs on the tails of core histones (histones H2A, H2B, H3 and H4), where it has roles in regulating gene expression [1]. Lysyl residues can undergo successive methylations on the $N^{\varepsilon}$-nitrogen to give three methylation states (mono-$N^{\varepsilon}$-methyllysine, di-$N^{\varepsilon}$-methyllysine and tri-$N^{\varepsilon}$-methyllysine respectively), as catalysed by *S*-adenosylmethionine-dependent methyltransferases (KMTs) [2,3]. In many cases, KMTs catalyse methylation at multiple sites to give different methylation states, on both histones and non-histone proteins [1,4]. Enzyme-catalysed demethylation of methylated lysyl residues also occurs at many sites on histones H3 and H4 [1]. Thus, at least at certain sites, lysyl methylation is dynamically regulated by the interplay between the two enzyme-catalysed processes.

Demethylation is catalysed by two families of histone lysine demethylases (KDMs) [5]. Members of the larger family of KDMs, JmjC KDMs, catalyse methyl group oxidation coupled to oxygen-dependent oxidative decarboxylation of 2-oxoglutarate (2OG), forming succinate and carbon dioxide (Fig. 1A) [5]. The available evidence implies that the resultant hemiaminal is normally unstable, fragmenting to give the demethylated lysyl residue and formaldehyde [6]. Dysregulation of JmjC KDM family members is implicated in many diseases, including developmental disorders and many cancers. The JmjC KDMs are thus the focus of drug development programmes [7], although their physiological roles are, in many cases, incompletely defined. There is emerging evidence that certain KDMs have multiple substrates including non-histone proteins and potentially methylated arginyl residues [8,9], suggesting the possibility for *in vivo* pleiotropy in KDM catalysis.

Though less well studied, lysyl methylation has been observed on histones other than H3 and H4. Histone 1

**Abbreviations**
2OG, 2-oxoglutarate; FDH, formaldehyde dehydrogenase; HP1, heterochromatin protein 1; KDM, histone lysine demethylase; KMT, S-adenosylmethionine-dependent methyltransferase; NOG, *N*-oxalylglycine.



FEBS Letters **592** (2018) 3264–3273 

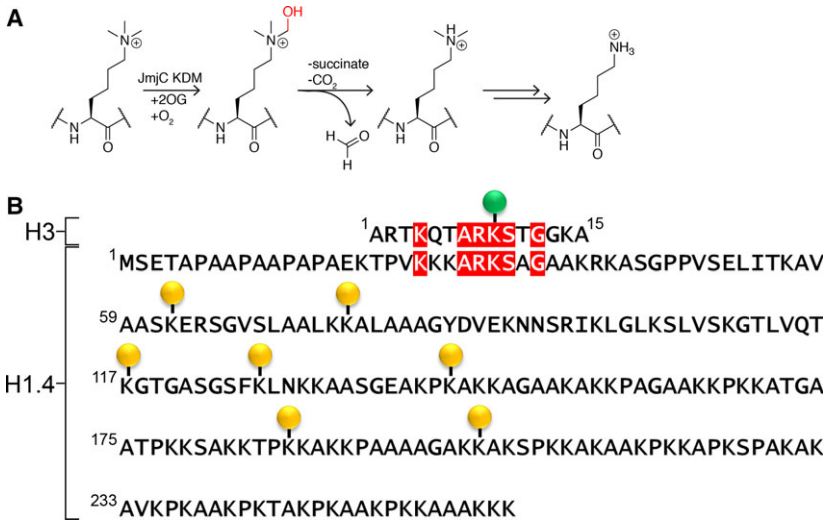


**Fig. 1.** Demethylation by the JmjC KDMs. (A) Outline mechanism of histone lysine demethylation as catalysed by the JmjC KDMs. (B) Sequence alignment of the first 15 residues of histone H3 with the sequence of histone H1.4. The H3K9 position known to be methylated is marked with a green circle. Other positions known to be methylated on H1.4 are marked with yellow circles [12,13,45].

isotype 4 (H1.4), as opposed to the core histones H2A, H2B, H3 and H4, is one of multiple 'linker' histones that bind to nucleosomal DNA, but which do not form part of the histone octamer [10]. Linker histones have been traditionally viewed as playing important structural roles in stabilising higher order chromatin structure [11]. More recent evidence suggests that histone 1 isotypes and their post-translational modifications also have additional functional roles within the cell, including in transcriptional regulation [11,12]. To date, a number of sites of histone H1.4 lysyl $N^{\epsilon}$-methylation have been identified (Fig 1B), with H1.4K26 being the most abundantly methylated site on H1.4 [13]. The methylation status of H1.4K26 is reported to vary dynamically during the cell cycle [14], and to undergo KDM4-catalysed demethylation, as supported by *in vitro* studies on mouse KDM enzymes [15]. The methylation status of the H1.4K26 residue is commonly associated with repressed genes, and is known to regulate binding of the family of heterochromatin protein 1 (HP1) proteins and related chromodomains, such as CDYL2 [16,17]. Loss of H1.4K26 (by substitution with a histone H1.4 variant bearing an alanine residue at this position, H1.4K26A) results in a reduction of cell proliferation, deregulation of gene expression and a reduction of stabilisation of H1.4 in heterochromatic regions [14]. Methylation of H1.4K26 also enhances phosphorylation of H1.4K27 by the Aurora B kinase, which in turn hinders recruitment of HP1 to H1.4K26me2 [17,18]. H1.4K26 is also reported to be acetylated by an unknown acetyltransferase, and to be deacetylated by SIRT1 [19]. Thus, emerging, and incompletely characterised, results indicate that complex regulatory loops exist for H1.4, in addition to those established with the core histones.

All human KDM4 enzymes catalyse demethylation of H3K9 methylation, with KDM4A-C additionally catalysing H3K36 demethylation [20–23]. Some KDM4 subfamily members have also been demonstrated to catalyse *in vitro* demethylation of $N^{\epsilon}$-methylated H3K27 and arginine residues in the H3 and H4 tails [8,24]. With respect to their activity on H1.4, it is currently unclear (a) how the demethylation efficiency at H1.4K26 compares to other KDM4 substrates (H3K9 and H3K36), (b) how the H1.4K26 substrate binds within KDM4 active sites, and also (c) whether JmjC KDMs other than the KDM4s can catalyse demethylation at H1.4K26.

To address these questions, we report studies investigating human JmjC KDM-catalysed demethylation of H1.4K26 methylation. Our findings reveal that demethylation of methylated lysyl residues in H1.4K26 peptide fragments is catalysed by all members of the human KDM4 subfamily of JmjC KDMs (KDM4A-E), supporting previously reported cell-based studies (predominantly with mouse enzymes) [15]. Unexpectedly, we also observed low level H1.4K26me2 demethylation activity by KDM7A and KDM7B (PHF8), in the context of fragment peptides, though at levels that may not be biologically relevant. While demethylation of H1.4K26me2/1-containing peptides is relatively inefficient for KDM7A and KDM7B, kinetic analyses indicate that H1.4K26me3 is a comparably efficient substrate for KDM4A as H3K9me3 (at least in the context of fragment peptides) and is a better substrate than H3K36me3. This assignment is supported by crystallographic studies indicating that the H1.4K26me3 peptide binds to the KDM4 active site in a similar manner to the H3K9me3 peptide. Overall, H1.4K26me3 appears to be a good substrate for KDM4A, and indeed other KDM4 enzymes, which is

supportive of its assignment as a KDM4 substrate in mouse and human cells [15].

## Materials and methods

### Protein production

The catalytic domains of the JmjC KDMs used in this work were recombinantly expressed as reported either in *Escherichia coli* ($KDM2A_{1–557}$ [25], $KDM4A_{1–359}$ [26], $KDM4B_{1–359}$, $KDM4C_{1–359}$, $KDM4D_{1–359}$, $KDM4E_{1–337}$ [27], $KDM6B_{1141–1590}$ [28], $KDM7B_{1–447}$ [29], $KDM7A_{38–480}$ [28]) or Sf9 cells ($KDM3A_{515–1317}$ [28], $KDM5C_{1–765}$ [28]) as N-terminally His6-tagged proteins. Proteins were purified by Ni-affinity chromatography followed by size exclusion chromatography as previously described.

### Peptide synthesis

Peptides were produced as C-terminal amides using a Liberty Blue automated microwave peptide synthesiser (CEM Corporation, Matthews, NC, USA), using standard fluorenylmethyloxycarbonyl-mediated solid-phase chemistry and NovaPEG rink amide resin (Merck, Kenilworth, NJ, USA). Following synthesis, peptides were cleaved from the resin by incubation with trifluoroacetic acid/water/triisopropylsilane/dimethoxybenzene (92.5 : 2.5 : 2.5 : 2.5) for 3 h followed by precipitation with ice-cold diethyl ether. For kinetic experiments, lyophilised peptides were purified by reverse-phase high-performance liquid chromatography using a Vydac C18 column (Solvent A: 0.1% trifluoroacetic acid in $H_2O$, Solvent B: 0.1% trifluoroacetic acid in acetonitrile). Sequences are given in Table S1.

### MALDI-TOF MS activity assays

Recombinant proteins (1 μM) were incubated with peptides (10 μM, sequences are given in Table S1) in 50 mM HEPES, pH 7.5 with addition of Fe(II) ammonium sulfate (10 μM), sodium ascorbate (100 μM) and 2-oxoglutaric acid (200 μM). Reactions with KDM3A and KDM7A also contained 1 mM tris(2-carboxyethyl)phosphine hydrochloride. No enzyme reactions were included as negative controls. Reactions were incubated for 1 h at 37 °C before being quenched with 1 : 1 (v/v) methanol. Analysis was carried out by MALDI-TOF MS (Bruker, Billerica, MA, USA), with demethylation observed as mass shifts of 14 Da.

### NMR activity assays

The NMR analyses employed a Bruker Avance III 700 MHz spectrometer with an inverse TCI cryoprobe optimised for $^1H$ observation and were carried out as previously described [6]. Samples (KDM4A (10 μM), 2OG (400 μM), H1.4(18–32) K26me3 peptide (400 μM), Fe(II) ammonium sulfate (100 μM) and ascorbate (1 mM) in 50 mM ammonium formate, pH 7.5, 500 mM NaCl in 10% v/v $D_2O$) were prepared in a microcentrifuge tube (total volume = 75 μL), before being transferred to an NMR tube. The samples were then analysed over time using automated routines; each timepoint corresponded to one experiment accumulating 16 transients (89 s total acquisition time per experiment). The solvent resonance was depleted by excitation sculpting using a 180° sinc pulse (duration = 2 ms) [30].

### Kinetic analyses

Kinetic parameters for KDM4 enzymes were determined by use of an FDH (formaldehyde dehydrogenase)/$NAD^+$-coupled) assay for quantification of the formaldehyde reaction byproduct, as previously described [27]. Assays were carried out in 50 mM HEPES, pH 7.5, 0.01% Tween-20, with addition of Fe (II) ammonium sulfate (10 μM), sodium ascorbate (100 μM), 2-oxoglutarate (200 μM), $NAD^+$ (500 μM), KDM4 enzymes (1 μM for specific activities, 500 nM for Michaelis–Menten kinetics) and FDH enzyme (0.001 $U{\cdot}\mu L^{-1}$, Sigma-Aldrich, St Louis, MO, USA) in a 30-μL volume in black 384-well plates. Specific activities were measured using a 100-μM peptide. For Michaelis–Menten experiments, peptide concentrations were varied. Reactions were monitored using a PHERAstar FS plate reader (BMG Labtech, Ortenberg, Germany) with 355 nm excitation and 460 nm emission. Kinetic parameters were calculated from the reaction rate during the initial linear phase of formaldehyde production, which were used to calculate specific activities or fitted to Michaelis–Menten equations using GRAPHPAD PRISM (GraphPad Software, La Jolla, CA, USA).

### X-ray crystallography

Co-crystals of $KDM4A_{1–359}$.Ni(II).H1.4(18–32)K26me3. NOG were obtained in sitting drops grown at 4 °C with a ratio of 1 : 2 sample to well solution [0.1 M MIB buffer (malonic acid/imidazole/boric acid, pH 6.0, 25% w/v PEG 1500)] [26]. Drops contained 10 $mg{\cdot}mL^{-1}$ KDM4A, 5 mM H1.4(18–32)K26me3, 5 mM NOG and 4 mM $NiCl_2$. Crystals were cryoprotected with 25% glycerol then flash-frozen in liquid $N_2$. Data were collected using a single crystal at 100 K at the Diamond I04-1 MX beam line and were processed with HKL2000 [31]. The structure was solved by molecular replacement using PHASER [32] (search model: PDB ID 2OX0) and was refined by alternative cycles of CNS [33] and PHENIX[34], with iterative rebuilding of the refined model using COOT [35]. All residues were in the allowed regions of the Ramachandran plot as calculated by PROCHECK [36]. Data collection and refinement statistics are given in Table S2. The crystal structure has been deposited under PDB accession code 6H8P.

## Results

The propensity of human JmjC KDMs to catalyse demethylation at H1.4K26 was investigated using

recombinant forms of the catalytic domains of representatives of each human JmjC KDM subfamily (KDM2-7) and fragment peptides (Table S1) [37]. Three peptides with identical sequences, corresponding to residues 18–32 of histone H1.4 ($H_2N$-TPVKKKA RKSAGAAK-$CONH_2$), but containing either a $N^{\varepsilon}$-tri-, di- or monomethyllysine at K26 were synthesised (Fig. 1B and Table S1). Activity assays monitoring JmjC KDM-catalysed demethylation of the peptides were then carried out; samples were prepared containing each peptide, 2-oxoglutarate (2OG), ferrous iron, ascorbate and individual representatives from each JmjC KDM subfamily (KDM2A [38], KDM3A [21], KDM4E [22], KDM5C [39,40], KDM6B [41], KDM7A [42]). After incubation for 1 h at 37 °C, matrix-assisted laser desorption ionisation mass spectrometry (MALDI-TOF MS) analysis revealed clear demethylation of all three H1.4 peptides containing $N^{\varepsilon}$-lysine methylation at K26 in samples containing KDM4E, consistent with previous *in vitro* and in cell studies with closely related subfamily member, KDM4D (Fig. 2A, Table 1 and Fig. S2) [15,43]. While no evidence for demethylation was observed in samples of any of the H1.4 peptides with KDM2A, KDM3A, KDM5C or KDM6B (Table 1, Figs S3–S6), low levels of demethylation (<10%) of the mono- and dimethylated H1.4K26 peptides were also observed in samples containing KDM7A (Table 1, Fig. S7).

Given the activity observed with KDM4E and KDM7A, we decided to investigate the intra-subfamily conservation of this demethylation activity. The demethylation activity of the other subfamily members (KDM4A-D and KDM7B) was therefore screened. For all KDM4 subfamily members, we observed H1.4K26 demethylation activity similar to that already observed with KDM4E (Table 1, Figs S8–S11); however, no H1.4K26 demethylation activity was observed with KDM7B at this enzyme concentration (Fig. S12). Note that as with H3K9, demethylation of the monomethylated H1.4K26 peptide was only observed with KDM4E, under the stated conditions [24].

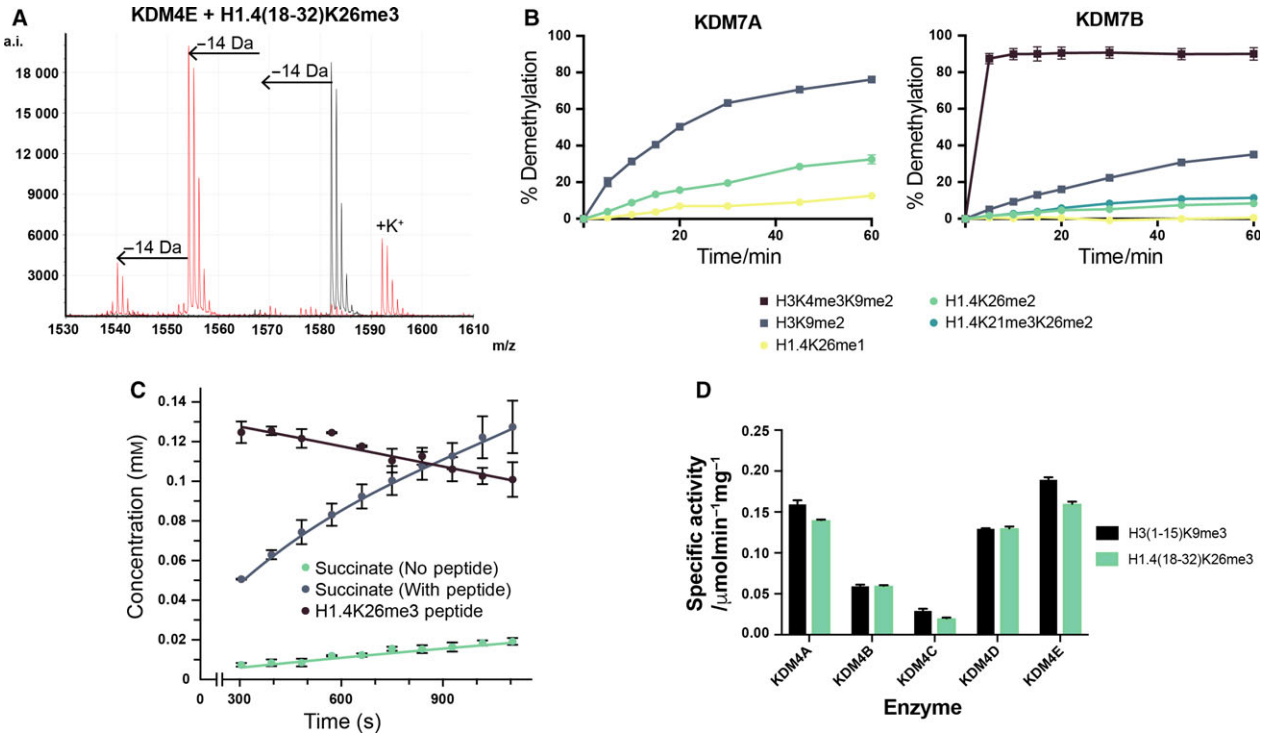


**Fig. 2.** H1.4K26 N-terminal demethylation is catalysed by JmjC KDMs. (A) Demethylation of an H1.4(18–32)K26me3 peptide by KDM4E. The red spectrum shows reactions containing enzyme; the black spectrum is a no enzyme control. (B) Comparison of activity of KDM7A and KDM7B on H1.4K26 and H3K9 methylated peptides. Time course experiments containing the stated enzyme (5 μM) and peptides (10 μM) were carried out at 37 °C, with samples removed and quenched at 8 time-points. Samples were analysed by MALDI-TOF MS. (C) Graphs showing the degree of succinate production and peptide demethylation of H1.4(18–32)K26me3 catalysed by KDM4A as quantified by $^1$H NMR (700 MHz). (D) Comparison of specific activity of KDM4 enzymes (1 μM) with H3(1–15)K9me3 and H1.4(18–32)K26me3 (100 μM). All data show the mean and standard deviation of technical triplicates.

**Table 1.** Summary of activity results for recombinant human JmjC KDMs on methylated H1.4 peptides. ● Indicates that clear demethylation activity was observed; ● Indicates that low level demethylation activity was observed (<10% conversion after 1 h); ● Indicates no activity under the stated conditions (1 μM KDM, 10 μM peptide); *Indicates demethylation activity was only observed with 5 μM KDM.

| Enzyme | H1.4(18–32) K26me1 | H1.4(18–32) K26me2 | H1.4(18–32) K26me3 |
|---|---|---|---|
| KDM2A | ● | ● | ● |
| KDM3A | ● | ● | ● |
| KDM4A | ● | ● | ● |
| KDM4B | ● | ● | ● |
| KDM4C | ● | ● | ● |
| KDM4D | ● | ● | ● |
| KDM4E | ● | ● | ● |
| KDM5C | ● | ● | ● |
| KDM6B | ● | ● | ● |
| KDM7A | ● | ● | ● |
| KDM7B | ●* | ●* | ● |

$N^{\varepsilon}$-Trimethylated H3K4 binds to the plant homeobox domain of KDM7B, targeting the $N^{\varepsilon}$-dimethyllysine at H3K9 to the catalytic domain, and thus promoting demethylation [29,44]. To test whether similar targeting may occur with H1.4, promoting activity at H1.4K26, an H1.4 peptide was synthesised containing *di*-$N^{\varepsilon}$-methyllysine at K26 and tri-$N^{\varepsilon}$-methyllysine at K21 (i.e. at the equivalent position in the sequence to K4 in the H3 peptide, Fig. 1B, Table S1). Monomethylation at H1.4K21 has previously been observed by proteomic mass spectrometry [45]. With the aim of enhancing activity, the enzyme concentration was increased from 1 μM to 5 μM, and time course analyses were conducted with both KDM7A and KDM7B, both with the new peptide (H1.4(18–32) K21me3K26me2) and the H1.4 peptides methylated only at K26 (Fig. 2B). At this increased enzyme concentration, clear evidence for demethylation of H1.4K26me2 was observed with KDM7B in addition to KDM7A (Fig. S12E), but no significant difference was observed between the peptide with and without methylation at H1.4K21 (Fig. 2B). Thus, it appears unlikely that $N^{\varepsilon}$-trimethylation at H1.4K21 promotes demethylation at H1.4K26 by KDM7B. These time courses, and similar ones with KDM7A, confirmed that the H1.4K26 peptides were significantly poorer substrates for the KDM7 subfamily than the H3K9 peptides (the weak demethylation efficiency observed for KDM7A/B precluded further kinetic analyses).

Studies then focused on determining the proficiency of H1.4K26 demethylation by the KDM4 enzymes. Specific activities of each enzyme with H1.4K26me3 were compared to those with H3K9me3, and more detailed studies were carried out with a representative KDM4 enzyme, KDM4A. $^{1}$H NMR time course analyses with KDM4A and the trimethylated H1.4K26me3 peptide confirmed time-dependent demethylation of the Kme3 residue (Figs 2C, S13). The $^{1}$H NMR experiments also revealed concomitant turnover of 2OG into succinate (emergence of a singlet $^{1}$H resonance at $\delta_H$ 2.28 ppm, Fig. S13) that is consistent with the proposed demethylation mechanism [5].

Kinetic analyses were then undertaken using a fluorescence-based formaldehyde dehydrogenase (FDH)-coupled demethylation assay, which monitors the formation of NADH during FDH-catalysed oxidation of formaldehyde [27]. Initially, specific activities for each KDM4 enzyme with either H1.4K26me3 or H3K9me3 (each at 100 μM) were determined for comparison (Figs 2D, S14). These results revealed that in all cases demethylation of the two different marks was roughly comparable.

Michaelis–Menten kinetics were then conducted with KDM4A. Samples containing KDM4A, 2OG, ascorbate, H1.4K26me3 peptide, $NAD^+$ and FDH were analysed over time and kinetic parameters were determined by recording the initial reaction rates of NADH production (corresponding to enzymatic production of formaldehyde) at varying peptide concentration. Similar experiments were carried out with H3K9me3 and H3K36me3 substrate peptides and the obtained values compared (Table 2). The experiments revealed that the H1.4K26me3 and H3K9me3 peptides are similarly efficient substrates of KDM4A, giving similar $K_M$ (32.3 ± 6.4 μM and 25.5 ± 4.9 μM respectively) and $k_{cat}$ (0.32 ± 0.049 $s^{-1}$ and 0.31 ± 0.045 $s^{-1}$ respectively) values. Demethylation of the H3K36me3 peptide was the least efficient, with higher $K_M$ (66.8 ± 5.4 μM) and lower $k_{cat}$ (0.12 ± 0.004 $s^{-1}$) values than with the other two peptides.

Crystallographic analyses were undertaken to investigate the binding mode of trimethylated H1.4K26 in

**Table 2.** Kinetic parameters for demethylation of H1.4 peptides by recombinant human KDM4A (1 μM) measured using a formaldehyde dehydrogenase-coupled demethylation assay [27]. Data show the mean and standard deviation of three independent replicates. See Materials and methods for complete assay conditions.

| | $K_M$/μM | $k_{cat}$/$s^{-1}$ | $k_{cat}/K_M$ |
|---|---|---|---|
| H3(1–15)K9me3 | 25.5 ± 4.9 | 0.31 ± 0.045 | 0.0124 |
| H1.4(18–32)K26me3 | 32.3 ± 6.4 | 0.32 ± 0.049 | 0.0098 |
| H3(29–43)K36me3 | 66.8 ± 5.4 | 0.12 ± 0.004 | 0.0019 |


FEBS Letters **592** (2018) 3264–3273 © 2018 The Authors. *FEBS Letters* published by John Wiley & Sons Ltd on behalf of Federation of European Biochemical Societies

the KDM4A active site. An X-ray crystal structure of a KDM4A:Ni(II):*N*-oxalylglycine:H1.4K26me3 peptide complex was solved to a resolution of 1.98 Å (Note: Ni(II) was used for crystallisation in place of the catalytically relevant Fe(II) due to its oxidative stability; *N*-oxalylglycine (NOG) is a 2OG mimetic inhibitor) [46]. Density was observed for H1.4 residues 24–29. Refinement revealed the H1.4K26me3 peptide bound in a cleft along the surface of KDM4A with the methylated K26 residue protruding towards the active site-bound metal centre (Figs 3A, S1), positioning the carbon of the methyl group ~4 Å from the active site metal, apparently productively poised for enzymatic hydroxylation and subsequent demethylation.

Comparison of the H1.4K26me3 complex structure with those for a KDM4A:Ni(II):NOG:H3K9me3 peptide complex (PDB: 2OQ6 [26], Fig. 3B) and a KDM4A:Ni(II):NOG:H3K36me3 peptide complex (PDB: 2P5B [47], Fig. 3C) reveals that all three peptides bind with the side chain of the trimethyllysine residue in the same orientation. All three peptides have the same N- to C- directionality through the active site. The two residues N-terminal to the trimethyllysine residue (A24, R25 in the H1.4 peptide, A7, R8 in the H3K9 peptide and G34, V35 in the H3K36 peptide) adopt a similar conformation/orientation in all three structures, with backbone hydrogen bonds between KDM4A E169 and the peptide residues at the −1 and −2 positions (Fig. 3B/C). However, differences arise in the conformations of the C-terminal regions of the peptides. The H3K9me3 and H1.4K26me3 peptides manifest similar conformations/orientations for the three residues C-terminal to the target trimethyllysine residue, sharing conserved interactions with KDM4A K241, D135 and N86 (black dashes, Fig. 3B). By contrast with the H3K9me$_n$ and H1.4K26me3 substrate structures, the peptide backbone of H3K36 adopts a more 'bent' conformation, likely enforced by the

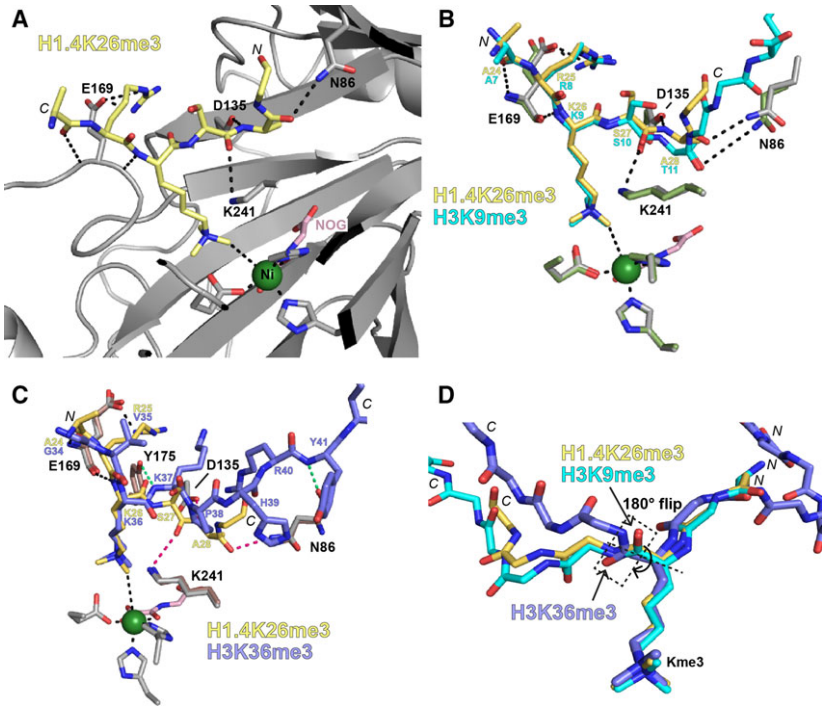


**Fig. 3.** Binding mode of H1.4K26me3 to KDM4A. The figure shows views from (A) an X-ray crystal structure of KDM4A bound to nickel (green, substitute for iron), NOG (pink, a 2OG mimetic inhibitor) and an H1.4(18–32)K26me3 peptide (yellow), alone, or overlaid with: (B) a structure of KDM4A bound to H3(7–14)K9me3 peptide (cyan, PDB ID 2OQ6) [26], and (C) a structure of KDM4A bound to an H3K36me3 peptide (violet, PDB ID 2P5B) [47]. Residues from KDM4A in the H1.4K26 structure are shown as pale grey sticks, those from KDM4A in the H3K9 structure are shown as pale green sticks and those from KDM4A in the H3K36 structure are shown as pale pink (A–C). Some of the key interactions between KDM4A and the H1.4K26me3 peptide are shown by black dashes. Interactions between the H1.4K26me3 peptide and KDM4A conserved in the H3K9me3 peptide structure, but not in the H3K36me3 peptide structure are marked as pink dashes. Interactions only observed in the H3K36me3 peptide structure are shown as green dashes. (D) Overlay of the peptide backbones (and Kme3 side chain) of each peptide. The amide flip between the H3K36 peptide, and the H3K9 and H1.4K26 peptides, is highlighted with a dashed black box.

presence of a proline (H3P38) in its sequence. Thus, in the K36 peptide, the backbone carbonyl of the H3K36 to K37 amide bond is 'flipped' ~180° compared to the analogous amide in the other two substrates (Fig. 3D). Unlike the H3K9 and H1.4K26 peptides (pink dashes, Fig. 3C), the H3K36 peptide displays no interactions with either KDM4A K241 or D135, nor with the side-chain of N86. Instead, the backbone –NH of the H3K36-K37 amide link interacts with the phenol of Y175 (green dashes, Fig. 3C).

Overall, the crystallographic analyses reveal the H1.4K26me3 substrate adopts a binding mode more similar to that of H3K9me3 than H3K36me3. This common binding geometry is supportive of their similar demethylation efficiencies.

## Discussion

Though lysyl methylations have been reported on linker histones [10,45], the processes that both regulate these methylation levels and contribute to their functional roles are largely undefined. Demethylation of methylated lysine residues at K26 of linker H1.4 has been reported to be catalysed by the KDM4 subfamily of JmjC KDMs in cells [15,43]. In previous studies on H1.4, no activity was observed for the KDM3 or KDM6 subfamilies; however, the KDM7 subfamily, which, like the KDM4s, also act at H3K9 had not been tested for activity with H1.4 [29,48,49]. Our results demonstrate that at least in the context of histone fragment peptides, recombinantly produced members of both the human KDM4 and KDM7 subfamilies of JmjC KDMs are capable of catalysing demethylation of methylated lysine residues at K26 of linker H1.4. Demethylation of dimethylated H1.4K26 by KDM7A and KDM7B appears considerably less efficient than the well-characterised H3K9me2 substrates for these enzymes, possibly precluding any biological relevance [29,42,44]. However, kinetic analyses with KDM4A reveal that demethylation of the H1.4K26me3 peptide and the well-characterised KDM4 H3K9me3 substrate are comparably efficient, whereas the H3K36me3 substrate is less efficiently demethylated than either H3K9me3 or H1.4K26me3 under the conditions tested [23,24,50,51].

Crystallographic analyses of H1.4K26me3 bound to KDM4A imply very similar binding modes for the H1.4K26me3 and an H3K9me3 peptides [26,47], consistent with the kinetic studies which imply that they are substrates of approximately equal efficiency. Importantly, the H3K36me3 peptide, which at least *in vitro* is a less efficient substrate for KDM4A-C (and not a substrate at all for KDM4D/E) than either H3K9me3 or H1.4K26me3, binds differently at the KDM4A active site [23,47,50]. One clear difference is in the binding mode of the amide bond on the C-terminal side of the *N*-methylated substrate lysine for H3K9/H1.4K26 versus H3K36 (Fig. 3). Although how this observation relates to the different binding/catalytic efficiencies of the different peptide sequences is difficult to dissect, it suggests that subtle differences in binding conformation may have substantial effects on catalytic efficiency, an observation relevant to functional assignment work on JmjC KDMs [50,52]. Similar subtleties have been observed for chromatin reader domains; in some cases they bind similarly to the closely related H3K9 and H1.4K26 sequences (e.g. HP1) [17], whilst in others binding is only observed to one or the other (e.g. ankyrin repeats of G9A) [43].

The combined biochemical and structural studies thus identify methylated H1.4K26 peptides as substrates for JmjC KDMs with broadly comparable demethylation efficiencies to those reported for KDM4 substrates on core histones [23,24,50,51]. Given this potential for activity at H1.4, it is of interest to further investigate the consequence of methylation at this position *in vivo*, in particular in the context of ongoing medicinal chemistry studies targeting the KDM4 subfamily as a treatment for disease [7,53]. The methylation status of H1.4K26 is reported to regulate binding of HP1 and other chromodomain proteins [16,17], which are associated with formation of heterochromatin. Thus, the reversal of this methylation by KDM4 enzymes in cells may well have direct effects on chromatin compaction and gene expression. It remains unclear whether a complex and dynamic 'histone code' akin to that proposed for the H3 N-terminal tail, exists for H1. The dynamic modulation of PTMs would be a likely requirement for this. Regulation of PTMs on H1.4 has already been demonstrated to play important roles in gene regulation, as in the case of acetylation of H1.4K34, which may help recruit the general transcription factor IID through its bromodomain, and which increases the dynamic exchange of H1 [54], or citrullination of H1.2R54, which results in histone eviction and chromatin decondensation [55]. The ready demethylation of H1.4K26 as catalysed by the KDM4 demethylase family argues that this might also be the case for H1.4K26 methylation, at least for H1.4K26me3 [12]. Overall, we hope that our findings will stimulate further cellular work to characterise the full scope of JmjC KDM substrate selectivity and will be informative for ongoing studies with JmjC KDM inhibitors.


FEBS Letters **592** (2018) 3264–3273 © 2018 The Authors. *FEBS Letters* published by John Wiley & Sons Ltd on behalf of Federation of European Biochemical Societies

## Acknowledgements

This work was supported by grants from Cancer Research UK (C8717/A18245), the Wellcome Trust (091857/7/10/7) and the Biotechnology and Biological Sciences Research Council. This project has received funding from the European Union's Horizon 2020 research and innovation programme under the Marie Skłodowska-Curie grant agreement No 657292 to LJW. RJH acknowledges a William R. Miller Junior Research Fellowship, St. Edmund Hall. AK acknowledges a Royal Society Dorothy Hodgkin Fellowship (DH120028), ERC Starting Grant (679479) and the Engineering and Physical Science Research Council (EP/L003376/1). JB acknowledges a studentship from the Engineering and Physical Science Research Council (EP/M508111/1). We thank Tristan Smart for purification of KDM2A, the Structural Genomics Consortium for providing KDM5C protein, Sarah Madden for KDM4A protein and Eidarus Salah for KDM4B and KDM4D protein.

## Author contributions

LJW, RJH, AK and CJS conceived the idea. AK and CJS supervised the study. LJW, RJH, YZ, JB and RS conducted experiments and analysed the results. RC carried out the crystallography. LJW, RJH and CJS wrote the manuscript. All authors critically reviewed the manuscript.

## References

1 Greer EL and Shi Y (2012) Histone methylation: a dynamic mark in health, disease and inheritance. *Nat Rev Genet* **13**, 343.
2 Hyun K, Jeon J, Park K and Kim J (2017) Writing, erasing and reading histone lysine methylations. *Exp Mol Med* **49**, e324-22.
3 Murn J and Shi Y (2017) The winding path of protein methylation research: milestones and new frontiers. *Nat Rev Mol Cell Biol* **18**, 517–527.
4 Zhang X, Wen H and Shi X (2012) Lysine methylation: beyond histones. *Acta Biochim Biophys Sin (Shanghai)* **44**, 14–27.
5 Walport LJ, Hopkinson RJ and Schofield CJ (2012) Mechanisms of human histone and nucleic acid demethylases. *Curr Opin Chem Biol* **16**, 525–534.
6 Hopkinson RJ, Hamed RB, Rose NR, Claridge TDW and Schofield CJ (2010) Monitoring the activity of 2-oxoglutarate dependent histone demethylases by NMR spectroscopy: direct observation of formaldehyde. *ChemBioChem* **11**, 506–510.
7 Johansson C, Tumber A, Che K, Cain P, Nowak R, Gileadi C and Oppermann U (2014) The roles of Jumonji-type oxygenases in human disease. *Epigenomics* **6**, 89–120.
8 Walport L, Hopkinson RJ, Chowdhury R, Schiller R, Ge W, Kawamura A and Schofield CJ (2016) Arginine demethylation is catalysed by a subset of JmjC histone lysine demethylases. *Nat Commun* **7**, 11974.
9 Li S, Ali S, Duan X, Liu S, Du J, Liu C, Dai H, Zhou M, Zhou L, Yang L *et al.* (2018) JMJD1B demethylates H4R3me2s and H3K9me2 to facilitate gene expression for development of hematopoietic stem and progenitor cells. *Cell Rep* **23**, 389–403.
10 Izzo A and Schneider R (2016) The role of linker histone H1 modifications in the regulation of gene expression and chromatin dynamics. *Biochim Biophys Acta – Gene Regul Mech.* **1859**, 486–495.
11 Fyodorov DV, Zhou BR, Skoultchi AI and Bai Y (2018) Emerging roles of linker histones in regulating chromatin structure and function. *Nat Rev Mol Cell Biol* **19**, 192–206.
12 Hergeth SP and Schneider R (2015) The H1 linker histones: multifunctional proteins beyond the nucleosomal core particle. *EMBO Rep* **16**, 1439–1453.
13 Lu A, Zougman A, Pudełko M, Bebenek M, Ziółkowski P, Mann M and Wiśniewski JR (2009) Mapping of lysine monomethylation of linker histones in human breast and its cancer. *J Proteome Res* **8**, 4207–4215.
14 Terme JM, Millán-Ariño L, Mayor R, Luque N, Izquierdo-Bouldstridge A, Bustillos A, Sampaio C, Canes J, Font I and Sima N (2014) Dynamics and dispensability of variant-specific histone H1 Lys-26/Ser-27 and Thr-165 post-translational modifications. *FEBS Lett* **588**, 2353–2362.
15 Trojer P, Zhang J, Yonezawa M, Schmidt A, Zheng H, Jenewein T and Reinberg D (2009) Dynamic histone H1 isotype 4 methylation and demethylation by histone lysine methyltransferase G9a/KMT1C and the Jumonji domain-containing JMJD2/KDM4 proteins. *J Biol Chem* **284**, 8395–8405.
16 Fischle W, Franz H, Jacobs SA, Allis CD and Khorasanizadeh S (2008) Specificity of the chromodomain Y chromosome family of chromodomains for lysine-methylated ARK(S/T) motifs. *J Biol Chem* **283**, 19626–19635.
17 Daujat S, Zeissler U, Waldmann T, Happel N and Schneider R (2005) HP1 binds specifically to Lys26-methylated histone H1.4, whereas simultaneous Ser27 phosphorylation blocks HP1 binding. *J Biol Chem* **280**, 38090–38095.
18 Hergeth SP, Dundr M, Tropberger P, Zee BM, Garcia BA, Daujat S and Schneider R (2011) Isoform-specific phosphorylation of human linker histone H1.4 in

mitosis by the kinase Aurora B. *J Cell Sci* **124**, 1623–1628.
19 Vaquero A, Scher M, Lee D, Erdjument-Bromage H, Tempst P and Reinberg D (2004) Human SirT1 interacts with histone H1 and promotes formation of facultative heterochromatin. *Mol Cell* **16**, 93–105.
20 Couture JF, Collazo E, Ortiz-Tello PA, Brunzelle JS and Trievel RC (2007) Specificity and mechanism of JMJD2A, a trimethyllysine-specific histone demethylase. *Nat Struct Mol Biol* **14**, 689–695.
21 Yamane K, Toumazou C, Tsukada Y, Erdjument-Bromage H, Tempst P, Wong J and Zhang Y (2006) JHDM2A, a JmjC-containing H3K9 demethylase, facilitates transcription activation by androgen receptor. *Cell* **125**, 483–495.
22 Whetstine JR, Nottke A, Lan F, Huarte M, Smolikov S, Chen Z, Spooner E, Li E, Zhang G, Colaiacovo M and Shi Y (2006) Reversal of lysine trimethylation by the JMJD2 family of histone demethylases. *Cell* **125**, 467–481.
23 Krishnan S and Trievel RC (2013) Structural and functional analysis of JMJD2D reveals molecular basis for site-specific demethylation among JMJD2 demethylases. *Structure* **21**, 98–108.
24 Williams ST, Walport LJ, Hopkinson RJ, Madden SK, Chowdhury R, Schofield CJ and Kawamura A (2015) Studies on the catalytic domains of multiple JmjC oxygenases using peptide substrates Studies on the catalytic domains of multiple JmjC oxygenases using peptide substrates. *Epigenetics* **9**, 1596–1603.
25 Rotili D, Altun M, Kawamura A, Wolf A, Fischer R, Leung IKH, Mackeen MM, Tian YM, Ratcliffe PJ, Mai A *et al.* (2011) A photoreactive small-molecule probe for 2-oxoglutarate oxygenases. *Chem Biol* **18**, 642–654.
26 Ng SS, Kavanagh KL, McDonough MA, Butler D, Pilka ES, Lienard BM, Bray JE, Savitsky P, Gileadi O, von Delft F *et al.* (2007) Crystal structures of histone demethylase JMJD2A reveal basis for substrate specificity. *Nature* **448**, 87–91.
27 Rose NR, Ng SS, Mecinović J, Liénard BM, Bello SH, Sun Z, McDonough MA, Oppermann U and Schofield CJ (2008) Inhibitor scaffolds for 2-oxoglutarate-dependent histone lysine demethylases. *J Med Chem* **51**, 7053–7056.
28 Rose NR, Woon EC, Tumber A, Walport LJ, Chowdhury R, Li XS, King ON, Lejeune C, Ng SS, Krojer T *et al.* (2012) Plant growth regulator daminozide is a selective inhibitor of human KDM2/7 histone demethylases. *J Med Chem* **55**, 6639–6643.
29 Loenarz C, Ge W, Coleman ML, Rose NR, Cooper CD, Klose RJ, Ratcliffe PJ and Schofield CJ (2010) PHF8, a gene associated with cleft lip/palate and mental retardation, encodes for an Nepsilon-dimethyl lysine demethylase. *Hum Mol Genet* **19**, 217–222.
30 Hwang T-L and Shaka AJ (1995) Water suppression that works. Excitation sculpting using arbitrary waveforms and pulsed field gradients. *J Magn Reson, Ser A* **112**, 275–279.
31 Otwinowski Z and Minor W (1997) Processing of X-ray diffraction data collected in oscillation mode. In Methods in Enzymology (Carter CW & Sweet RM, eds), pp. 307–326. Academic Press, New York, NY.
32 McCoy AJ, Grosse-Kunstleve RW, Adams PD, Winn MD, Storoni LC and Read RJ (2007) Phaser crystallographic software. *J Appl Crystallogr* **40**, 658–674.
33 Brünger AT, Adams PD, Clore GM, DeLano WL, Gros P, Grosse-Kunstleve RW, Jiang JS, Kuszewski J, Nilges M, Pannu NS *et al.* (1998) Crystallography & NMR System: A New Software Suite for Macromolecular Structure Determination. *Acta Crystallogr Sect D* **54**, 905–921.
34 Adams PD, Afonine PV, Bunkóczi G, Chen VB, Davis IW, Echols N, Headd JJ, Hung LW, Kapral GJ, Grosse-Kunstleve RW *et al.* (2010) PHENIX: a comprehensive Python-based system for macromolecular structure solution. *Acta Crystallogr Sect D* **66**, 213–221.
35 Emsley P, Lohkamp B, Scott WG and Cowtan K (2010) Features and development of Coot. *Acta Crystallogr Sect D* **D66**, 486–501.
36 Laskowski RA, MacArthur MW, Moss DS and Thornton JM (1993) PROCHECK: a program to check the stereochemical quality of protein structures. *J Appl Crystallogr* **26**, 283–291.
37 Klose RJ, Kallin EM and Zhang Y (2006) JmjC-domain-containing proteins and histone demethylation. *Nat Rev Genet* **7**, 715–727.
38 Tsukada Y, Fang J, Erdjument-Bromage H, Warren ME, Borchers CH, Tempst P and Zhang Y (2006) Histone demethylation by a family of JmjC domain-containing proteins. *Nature* **439**, 811–816.
39 Klose RJ, Yan Q, Tothova Z, Yamane K, Erdjument-Bromage H, Tempst P, Gilliland DG, Zhang Y and Kaelin WG Jr (2007) The Retinoblastoma Binding Protein RBP2 Is an H3K4 Demethylase. *Cell* **128**, 889–900.
40 Iwase S, Lan F, Bayliss P, de la Torre-Ubieta L, Huarte M, Qi HH, Whetstine JR, Bonni A, Roberts TM and Shi Y (2007) The X-linked mental retardation gene SMCX/JARID1C defines a family of histone H3 lysine 4 demethylases. *Cell* **128**, 1077–1088.
41 Lan F, Bayliss PE, Rinn JL, Whetstine JR, Wang JK, Chen S, Iwase S, Alpatov R, Issaeva I, Canaani E *et al.* (2007) A histone H3 lysine 27 demethylase regulates animal posterior development. *Nature* **449**, 689–694.

42 Tsukada Y, Ishitani T and Nakayama KI (2010) KDM7 is a dual demethylase for histone H3 Lys 9 and Lys 27 and functions in brain development. *Genes Dev* **24**, 432–437.
43 Weiss T, Hergeth S, Zeissler U, Izzo A, Tropberger P, Zee BM, Dundr M, Garcia BA, Daujat S and Schneider R (2010) Histone H1 variant-specific lysine methylation by G9a/KMT1C and Glp1/KMT1D. *Epigenetics Chromatin* **3**, 1–13.
44 Horton JR, Upadhyay AK, Qi HH, Zhang X, Shi Y and Cheng X (2010) Enzymatic and structural insights for substrate specificity of a family of jumonji histone lysine demethylases. *Nat Struct Mol Biol* **17**, 38–43.
45 Tweedie-Cullen RY, Brunner AM, Grossmann J, Mohanna S, Sichau D, Nanni P, Panse C and Mansuy IM (2012) Identification of combinatorial patterns of post-translational modifications on individual histones in the mouse brain. *PLoS ONE* **7**, e36980.
46 Hamada S, Kim TD, Suzuki T, Itoh Y, Tsumoto H, Nakagawa H, Janknecht R and Miyata N (2009) Synthesis and activity of N-oxalylglycine and its derivatives as Jumonji C-domain-containing histone lysine demethylase inhibitors. *Bioorg Med Chem Lett* **19**, 2852–2855.
47 Chen Z, Zang J, Kappler J, Hong X, Crawford F, Wang Q, Lan F, Jiang C, Whetstine J, Dai S *et al.* (2007) Structural basis of the recognition of a methylated histone tail by JMJD2A. *Proc Natl Acad Sci USA* **104**, 10818–10823.
48 Zhu Z, Wang Y, Li X, Wang Y, Xu L, Wang X, Sun T, Dong X, Chen L, Mao H *et al.* (2010) PHF8 is a histone H3K9me2 demethylase regulating rRNA synthesis. *Cell Res* **20**, 794–801.
49 Qiu J, Shi G, Jia Y, Li J, Wu M, Li J, Dong S and Wong J (2010) The X-linked mental retardation gene PHF8 is a histone demethylase involved in neuronal differentiation. *Cell Res* **20**, 908–918.
50 Hillringhaus L, Yue WW, Rose NR, Ng SS, Gileadi C, Loenarz C, Bello SH, Bray JE, Schofield CJ and Oppermann U (2011) Structural and evolutionary basis for the dual substrate electivity of the human KDM4 histone demethylase family. *J Biol Chem* **286**, 41616–41625.
51 Shiau C, Trnka MJ, Bozicevic A, Ortiz Torres I, Al-Sady B, Burlingame AL, Narlikar GJ and Fujimori DG (2013) Reconstitution of Nucleosome Demethylation and Catalytic Properties of a Jumonji Histone Demethylase. *Cell Chem Biol* **20**, 494–499.
52 Chen Z, Zang J, Whetstine J, Hong X, Davrazou F, Kutateladze TG, Simpson M, Mao Q, Pan CH, Dai S *et al.* (2006) Structural insights into histone demethylation by JMJD2 family members. *Cell* **125**, 691–702.
53 McAllister TE, England KS, Hopkinson RJ, Brennan PE, Kawamura A and Schofield CJ (2016) Recent Progress in Histone Demethylase Inhibitors. *J Med Chem* **59**, 1308–1329.
54 Kamieniarz K, Izzo A, Dundr M, Tropberger P, Ozretic L, Kirfel J, Scheer E, Tropel P, Wisniewski JR, Tora L *et al.* (2012) A dual role of linker histone H1. 4 Lys 34 acetylation in transcriptional activation. *Genes Dev* **26**, 797–802.
55 Christophorou MA, Castelo-Branco G, Halley-Stott RP, Oliveira CS, Loos R, Radzisheuskaya A, Mowen KA, Bertone P, Silva JC, Zernicka-Goetz M *et al.* (2014) Citrullination regulates pluripotency and histone H1 binding to chromatin. *Nature* **507**, 104–108.

## Supporting information

Additional supporting information may be found online in the Supporting Information section at the end of the article.

**Fig. S1.** Stereoview from a KDM4A.Ni.NOG.H1.4(18-32)K26me3 crystal structure.

**Fig. S2.** KDM4E catalyses lysine demethylation at H1.4K26.

**Fig. S3.** KDM2A does not catalyse lysine demethylation at H1.4K26 under the tested conditions.

**Fig. S4.** KDM3A does not catalyse lysine demethylation at H1.4K26 under the tested conditions.

**Fig. S5.** KDM5C does not catalyse lysine demethylation at H1.4K26 under the tested conditions.

**Fig. S6**. KDM6B does not catalyse lysine demethylation at H1.4K26 under the tested conditions.

**Fig. S7.** KDM7A catalyses lysine demethylation at H1.4K26.

**Fig. S8.** KDM4A catalyses lysine demethylation at H1.4K26.

**Fig. S9.** KDM4B catalyses lysine demethylation at H1.4K26.

**Fig. S10.** KDM4C catalyses lysine demethylation at H1.4K26.

**Fig. S11.** KDM4D catalyses lysine demethylation at H1.4K26.

**Fig. S12.** PHF8/KDM7B only catalyses lysine demethylation at H1.4K26 at high concentration.

**Fig. S13.** Analysis of KDM4A demethylation by $^{1}$H NMR.

**Fig. S14.** Specific activity determination for KDM4 enzymes.

**Table S1.** Peptide sequences used in this study.

**Table S2.** Crystallographic data processing and refinement statistics.